Supporting Information

Phonon-assisted electronic states modulation of few-layer $PdSe_2$ at terahertz frequencies

Ziqi Li[1†], Bo Peng[2†], Miao-Ling Lin[3], Yu-Chen Leng[3], Bin Zhang[1], Chi Pang[1], Ping-Heng Tan[3,*], Bartomeu Monserrat[2,4,*], and Feng Chen[1,*]

[1]School of Physics, State Key Laboratory of Crystal Materials, Shandong University, Shandong, Jinan, 250100, China.

[2]Cavendish Laboratory, University of Cambridge, J. J. Thomson Avenue, Cambridge CB3 0HE, United Kingdom.

[3]State Key Laboratory of Superlattices and Microstructures, Institute of Semiconductors, Chinese Academy of Sciences, Beijing 100083, China.

[4]Department of Materials Science and Metallurgy, University of Cambridge, 27 Charles Babbage Road, Cambridge CB3 0FS, United Kingdom.

†These authors contributed equally to this work.

Keywords: 2D materials, noble-transition-metal dichalcogenides, terahertz devices, phonon-assisted optical process, femtosecond spectroscopy.

Corresponding Author

*E-mails: drfchen@sdu.edu.cn; bm418@cam.ac.uk; phtan@semi.ac.cn.

Table of Contents

Supplementary Note 1: Tauc plot

To get more insight into the electronic band structure, the Tauc plot is derived with interband absorption theory[1]. The transition probability of the material can be calculated by:

$$A = \frac{4\pi\sigma_{\min}}{nc\Delta E_t} \tag{1}$$

where the $\sigma_{\min}$ is the minimum metallic conductivity, n represents the refractive index, and c is the velocity of light, and ΔE_t is the band tailing. It is assumed that the transition coefficient $r = ½$ for direct allowed and $r = 2$ for indirect allowed transitions. The bandgap of thin film sample can be derived as follows:

$$\alpha = \frac{A}{h\nu} \cdot \left(h\nu - E_g\right)^r \tag{2}$$

$$(\alpha h\nu)^{\frac{1}{r}} = A\left(h\nu - E_g\right) \tag{3}$$

where α is the absorption coefficient and can be calculated as (2.303Abs) / h_{8L}, in which the absorbance (Abs) is obtained as Abs = $\log_{10}(I_0/I)$ by UV-Vis-NIR Spectrophotometer and h_{8L} is the thickness measured by AFM results, and $h\nu$ is the incident photon energy. As can be seen from the formula, the extrapolation of the plotted line intercepts the $h\nu$ axis at the value of the indirect bandgap (Supplementary Fig. 1).

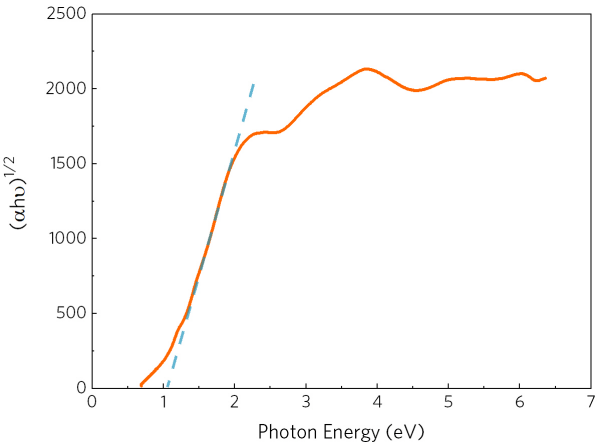

Supplementary Fig. 1. Tauc plot of CVD-grown $PdSe_2$ sample. The optical bandgap can be determined as the intersection of the linear rise of the plot with the baseline.

Supplementary Note 2: Thin film approximation

Here in this work, the differential transmittance $\Delta T/T$ is recorded by measuring the intensity of the electromagnetic wave through the sample with equilibrium or nonequilibrium states at different time delays. In the experiments, we first correct the data by using two identical substrates, so that the reflections and absorptions from the substrates are excluded. In addition, for the transmission modes of the thin film materials, their reflections are relatively small, so that the signal can be approximated as dominated by exciton absorption. For transparent thin films, both real and imaginary parts contribute to the absorption change. For transmission mode, the real part has negligible effects and the differential transmittance signal mainly depends on the imaginary part of the dielectric function.

For light propagation in matter, the electric field is

$$\vec{E}(r,t) = \vec{E}_0 e^{i\omega(\frac{n}{c}r-t)} = \vec{E}_0 e^{-\frac{2\pi k}{\lambda}r} e^{i\omega(\frac{n}{c}r-t)} \tag{9}$$

The complex refractive index is

$$\tilde{n} = n + ik \tag{10}$$

The light intensity is

$$I = \frac{1}{2}\varepsilon_0 cEE^* = \frac{1}{2}\varepsilon_0 cE_0^2 e^{-\frac{4\pi k}{\lambda}r} \tag{11}$$

In this work, we monitor the transient dynamics by measuring the incident intensity and transmitted intensity, and the change of its intensity is mainly related to the change of its imaginary part, represented as the product of the electric field and its complex conjugate. Strictly speaking, we should consider both the reflection and transmission of the sample at the same time. However, different from transient reflection measurement, we use transmission mode in which the influence of reflectivity of thin films is much lower. Therefore, the absorption can be approximately estimated as follows

$$\Delta A = -\log \frac{I_{pump+probe} - I_{probe}}{I_{probe}} \quad (12)$$

where I_0 is the intensity of the probe beam incident on the sample, and $I_{pump+probe}$ and I_{probe} are the intensity of the probe beam transmitted through the sample with and without the pump beam, respectively. In combination with the equilibrium absorptance Abs of the $PdSe_2$ sample by using UV–vis–NIR spectrophotometer (Agilent, Carry 5000), the absorptance spectrum at different pump-probe time delays can be further obtained. The exciton resonance energy can be therefore fitted with the transient absorptance Abs with Lorentzian fit.

Supplementary Note 3: Optical properties under different screening conditions

A high density of carriers leads to a significant increase in screening. As a result, the interaction between electrons decreases from the long-range Coulomb $1/r$ interaction to a shorter-range interaction. Because of the complex out-of-equilibrium processes including carrier-carrier scattering, electron-phonon coupling and various recombination pathways over different timescales, we choose a simple approximation by computing the Thomas-Fermi screening length in 2D $k_F = \sqrt{2\pi N_c}$, where N_c is the carrier density, and then use the screened Coulomb potential to mimic strong and weak screening conditions[2,3].

As shown in Supplementary Fig. 2, the screening length of 0.2 A^{-1} corresponds to a moderate photoexcited carrier density of 6.4×10^{13} cm^{-2}, and infinitely large screening length corresponds to a much stronger excitation. Hybrid functional uses a screened Coulomb potential to separate the short-range and long-range interactions, and with a screening length of 0.2 A^{-1} in the HSE06 hybrid functional to screen the long-range part of the Hartree-Fock exchange[3] can provide partial information of the band gap renormalization under moderate excitation. On the other hand, for strong screening, the screening length is infinitely large due to much higher photoexcited carrier density, which corresponds to the semilocal PBE functional as the long-range Coulomb interaction is fully screened in that case.

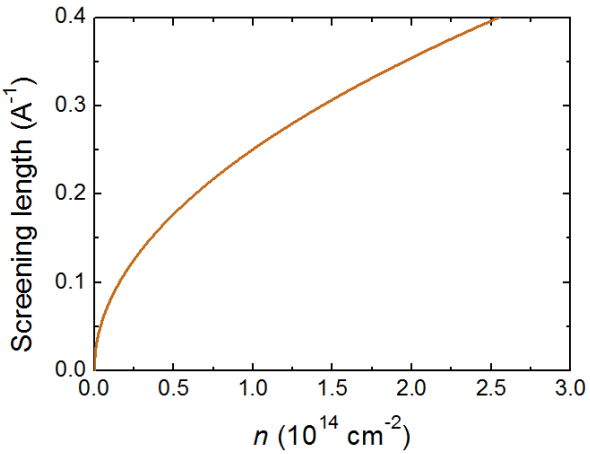

Supplementary Fig. 2. Screening length as a function of photoexcited carrier density based on Thomas-Fermi model in 2D.

The quasiparticle lifetime can be calculated from the imaginary part of the G_0W_0 self-energy[4,5], and the quasiparticle lifetimes for strong screening are much shorter than those for weak screening. The Bethe-Salpeter equation (BSE) on top of G_0W_0 self–energy corrections for both strong and weak screening conditions is employed to address the excitonic effects[6-8]. For BSE calculations, 96 valence bands and 96 conduction bands are included to compute the dielectric function.

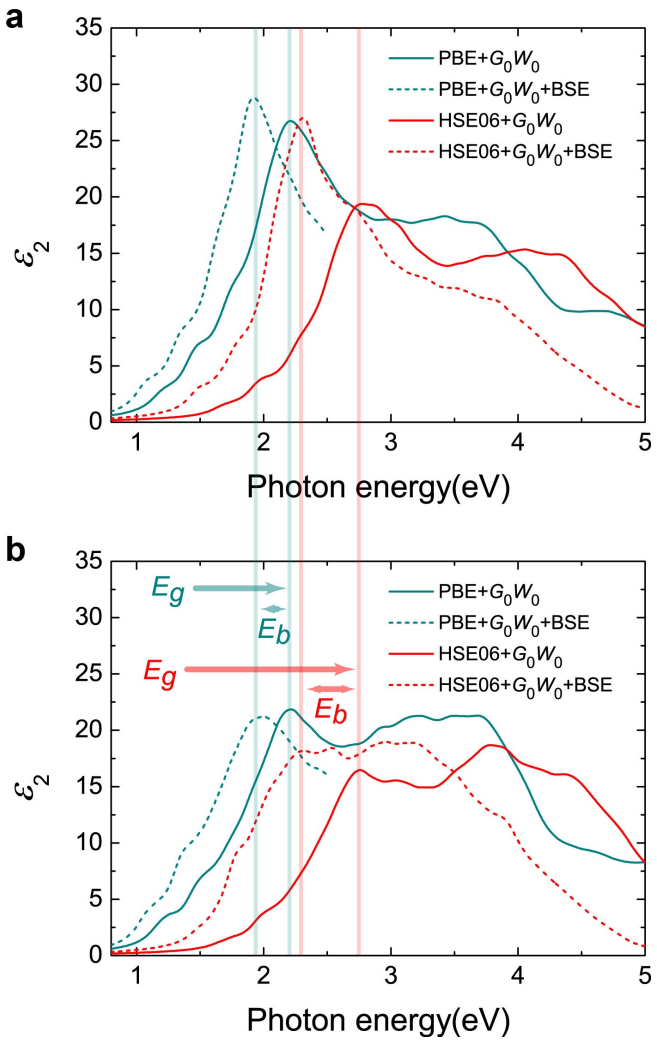

Supplementary Fig. 3. Calculated imaginary part of the dielectric function under weak (HSE06+G_0W_0) and strong screening conditions (PBE+G_0W_0) for polarization along (a) *a* and (b) *b* directions with and without the excitonic effects calculated from BSE. For A exciton of $PdSe_2$, the decrease of E_g is much larger than the decrease of E_b.

We note that a full description of non-equilibrium dynamics would require calculations based on non-equilibrium Green's function [9-12], but these calculations would be computationally prohibitive in a system as large as eight-layer $PdSe_2$ (even HSE06 and G_0W_0 calculations for eight-layer $PdSe_2$ are extremely time consuming).

Supplementary Note 4: Fourier transformation

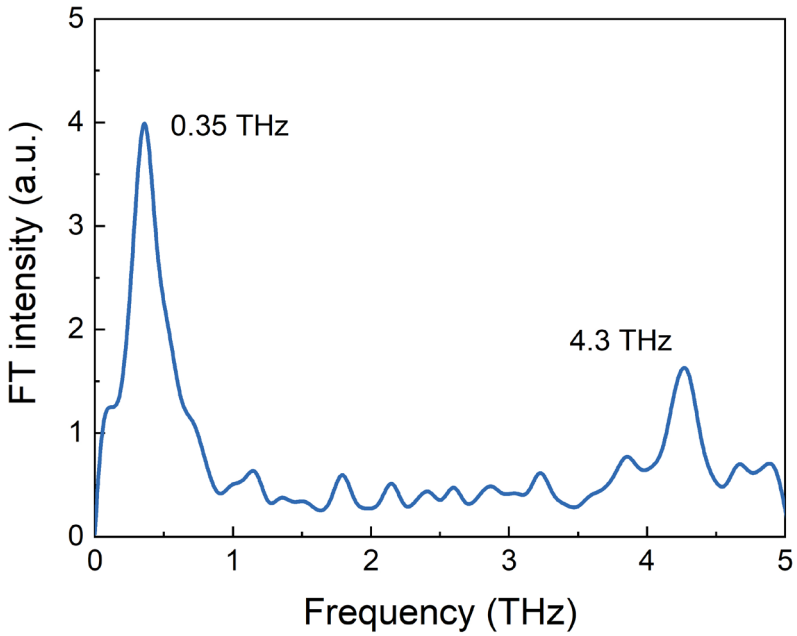

Supplementary Fig. 4. Fourier transform (FT) spectrum of the time-domain oscillations.

Supplementary Note 5: Lattice dynamics and electron-phonon coupling

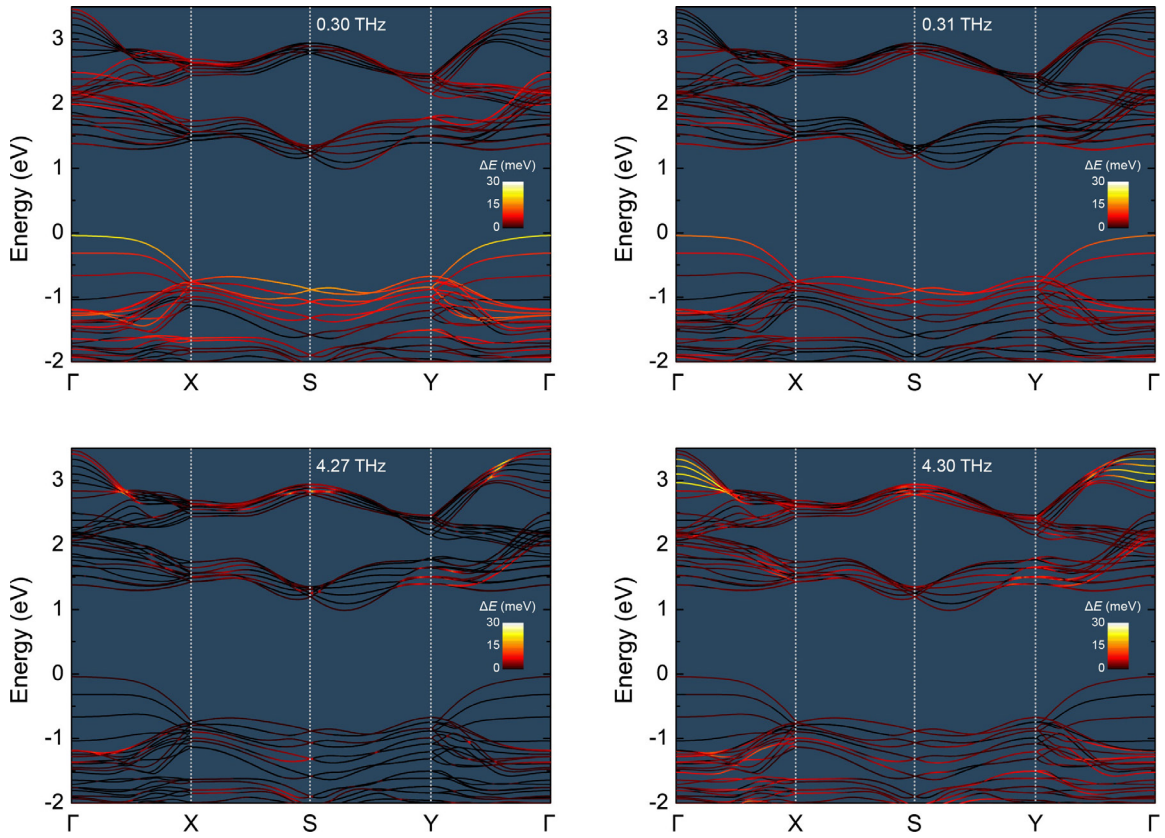

Supplementary Fig. 5. Electron-phonon coupling strength for different phonon modes at the Γ point.

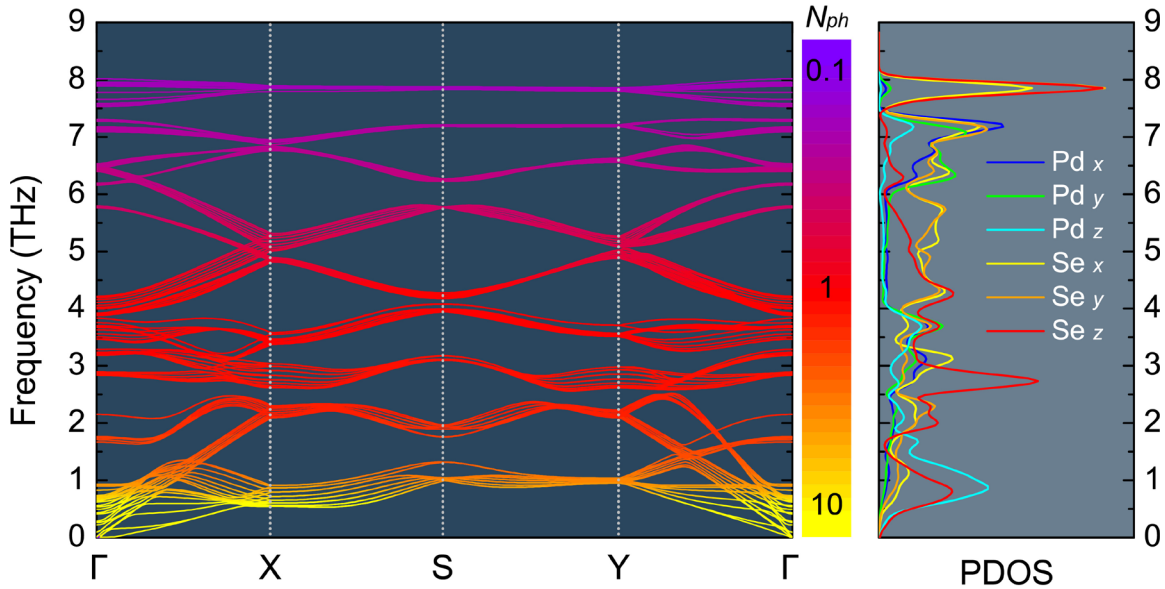

Supplementary Fig. 6. Full phonon dispersion of eight-layer $PdSe_2$ as well as the projected phonon density of states.

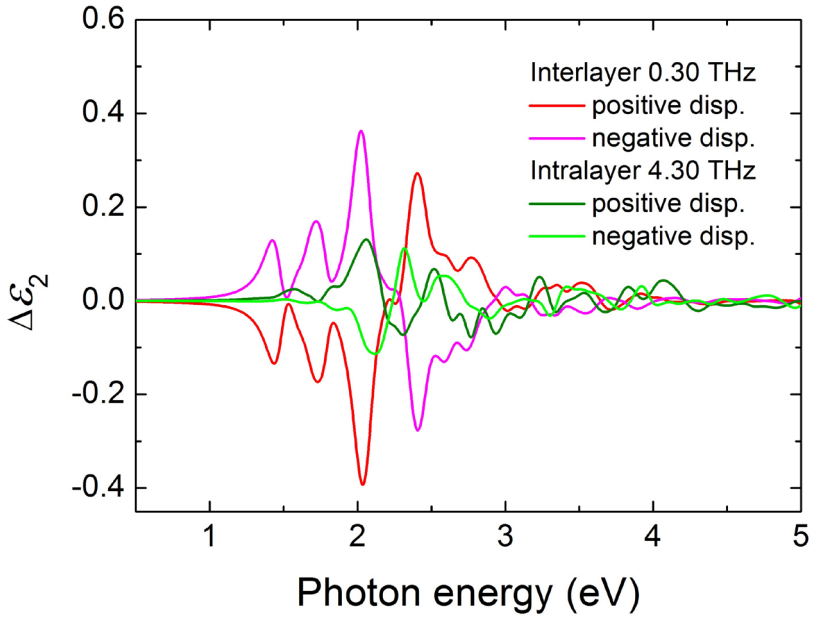

Supplementary Fig. 7. Change of the imaginary part of dielectric function under intralayer and interlayer phonon displacements calculated from HSE06+G_0W_0+BSE. Both positive and negative phonon displacements are included.

Supplementary References

1. Tauc, J. *Amorphous and liquid semiconductors*. (Springer Science & Business Media, 2012).

2. Nilforoushan, N. et al. Photoinduced renormalization of Dirac states in $BaNiS_2$. *Phys. Rev. Research* 2, 043397, (2020).

3. Jochen, H. & Gustavo, E. S. Hybrid functionals based on a screened Coulomb potential. *J. Chem. Phys.* **118**, 8207, (2003).

4. Marini, A., Del Sole, R., Rubio, A. & Onida, G. Quasiparticle band-structure effects on the d hole lifetimes of copper within the GW approximation. *Phys. Rev. B* **66**, 161104, (2002).

5. Nechaev, I. A., Zhukov, V. P. & Chulkov, E. V. Ab initio calculation of the lifetime of quasiparticle excitations in transition metals within the framework of the GW approximation. *Phys. Solid State* **49**, 1811–1819, (2007).

6. Albrecht, S., Reining, L., Del Sole, R. & Onida, G. Ab initio calculation of excitonic effects in the optical spectra of semiconductors. *Phys. Rev. Lett.* **80**, 4510–4513, (1998).

7. Rohlfing, M. & Louie, S. G. Electron-hole excitations in semiconductors and insulators. *Phys. Rev. Lett.* **81**, 2312–2315, (1998).

8. Sander, T., Maggio, E. & Kresse, G. Beyond the Tamm-Dancoff approximation for extended systems using exact diagonalization. *Phys. Rev. B* **92**, 045209, (2015).

9. Perfetto, E., Sangalli, D., Palummo, M., Marini, A. & Stefanucci, G. First-principles nonequilibrium green's function approach to ultrafast charge migration in glycine. *J. Chem. Theory Comput.* **15**, 4526–4534, (2019).

10. Perfetto, E. & Stefanucci, G. CHEERS: a tool for correlated hole-electron evolution from real-time simulations. *J. Phys.: Condens. Matter.* **30**, 465901, (2018).

11. Tuovinen, R., Golež, D., Eckstein, M. & Sentef, M. A. Comparing the generalized Kadanoff-Baym ansatz with the full Kadanoff-Baym equations for an excitonic insulator out of equilibrium. *Phys. Rev. B* **102**, 115157, (2020).

12. Attaccalite, C., Grüning, M. & Marini, A. Real-time approach to the optical properties of solids and nanostructures: Time-dependent Bethe-Salpeter equation. *Phys. Rev. B* **84**, 245110, (2011).